Catalysis Communications 24 (2012) 38–43

Contents lists available at SciVerse ScienceDirect

Catalysis Communications

journal homepage: www.elsevier.com/locate/catcom

Short Communication

NO selective reduction by hydrogen over bimetallic Pd–Ir/TiO_2 catalyst

Jia Li, Guangjun Wu, Naijia Guan, Landong Li *

Key Laboratory of Advanced Energy Materials Chemistry (Ministry of Education), College of Chemistry, Nankai University, Tianjin 300071, PR China

ARTICLE INFO

Article history:
Received 18 January 2012
Received in revised form 26 February 2012
Accepted 12 March 2012
Available online 20 March 2012

Keywords:
H_2-SCR
Pd–Ir/TiO_2
Bimetallic catalyst
XPS
FTIR

ABSTRACT

TiO_2 supported monometallic and bimetallic catalysts were prepared and employed in the selective catalytic reduction of nitrogen oxides by hydrogen (H_2-SCR). Bimetallic Pd–Ir/TiO_2 exhibited high activity in H_2-SCR reaction and NO_x conversion of >80%, with N_2 selectivity >80%, could be obtained in the temperature range of 413–473 K. The existence states of supported metals before and after H_2-SCR were investigated by X-ray photoelectron spectroscopy, and the surface species formed during H_2-SCR reaction were monitored by in situ FTIR spectroscopy. Based on the catalytic and characterization results, the synergistic effects between Pd and Ir were discussed and the H_2-SCR reaction pathways over Pd–Ir/TiO_2 were proposed.

1. Introduction

The selective catalytic reduction (SCR) is a promising technique for nitrogen oxides (NO_x) abatement in excess oxygen. Ammonia is the most familiar reducing agents employed in NO_x reduction and the selective catalytic reduction of NO_x by ammonia (NH_3-SCR) is well-known process for NO_x emission control from stationary sources [1,2]. Compared to ammonia, hydrogen is more feasible reducing agent for SCR reaction, because hydrogen is less processed and non-corrosive. Therefore, the selective catalytic reduction of NO_x by hydrogen (H_2-SCR) attracts great attention as alternative deNO_x route to NH_3-SCR. Most recently, a comprehensive review on current H_2-SCR researches has been presented by Costa et al. [3]. Supported noble metal catalysts, e.g. Pt catalysts [4–10] and Pd catalysts [11–14], are reported to be active in H_2-SCR. Despite of significant achievements achieved so far, a breakthrough of H_2-SCR technique is still hindered by the insufficient performances of catalysts.

Supported bimetallic catalysts have received considerable attention in the past decades. Due to the formation of synergistic effects between two metallic components, the activity of bimetallic catalyst may be greater than the sum of two separated monometallic catalysts. For example, bimetallic AuRh/Al_2O_3 has been proven to be good catalyst for the selective catalytic reduction of NO by propylene [15].

In this work, TiO_2 supported monometallic and bimetallic catalysts are studied for H_2-SCR reaction. The bimetallic Pd–Ir/TiO_2 catalyst exhibits much higher H_2-SCR activity than monometallic Pd/TiO_2 and Ir/TiO_2.

2. Experimental

2.1. Catalyst preparation

Commercial TiO_2 Degussa P25 was used as support and the supported monometallic catalyst was prepared via chemical reduction process. In a typical preparation of Pd/TiO_2, 2 g of TiO_2 and 50 mL of 2 mM $PdCl_2$ solution were added into 50 mL deionized water and dispersed by ultrasonic vibration. Then 10 mL of 1 M KBH_4 was dropwise added to the dispersion under the protection of nitrogen. The particles were filtered, dried and calcined in flowing He at 573 K for 2 h. Ir/TiO_2 and Rh/TiO_2 were prepared via similar processes. Bimetallic Pd–Ir/TiO_2 and Pd–Rh/TiO_2 were prepared by coinstantaneous chemical reduction processes and a mixture of bimetallic precursor was used instead of single metallic precursor.

2.2. Catalyst characterization

Transmission electron microscopy (TEM) images were acquired on a Tecnai G2 20 S-TWIN transmission electron microscope at an accelerate voltage of 200 kV.

X-ray photoelectron spectra (XPS) were recorded on a Kratos Axis Ultra DLD spectrometer with a monochromated Al–Ka X-ray source (hν = 1486.6 eV) and delay line detector (DLD). Accurate binding energies (±0.1 eV) were determined with respect to the position of the adventitious C 1s peak at 284.8 eV.

2.3. Catalyst testing

The H_2-SCR reaction at atmospheric pressure was performed in a fixed-bed flow micro-reactor. The total flow of the inlet gas was set

* Corresponding author. Tel./fax: +86 22 2350 0341.
E-mail address: lild@nankai.edu.cn (L. Li).

1566-7367/$ – see front matter © 2012 Elsevier B.V. All rights reserved.
doi:10.1016/j.catcom.2012.03.014

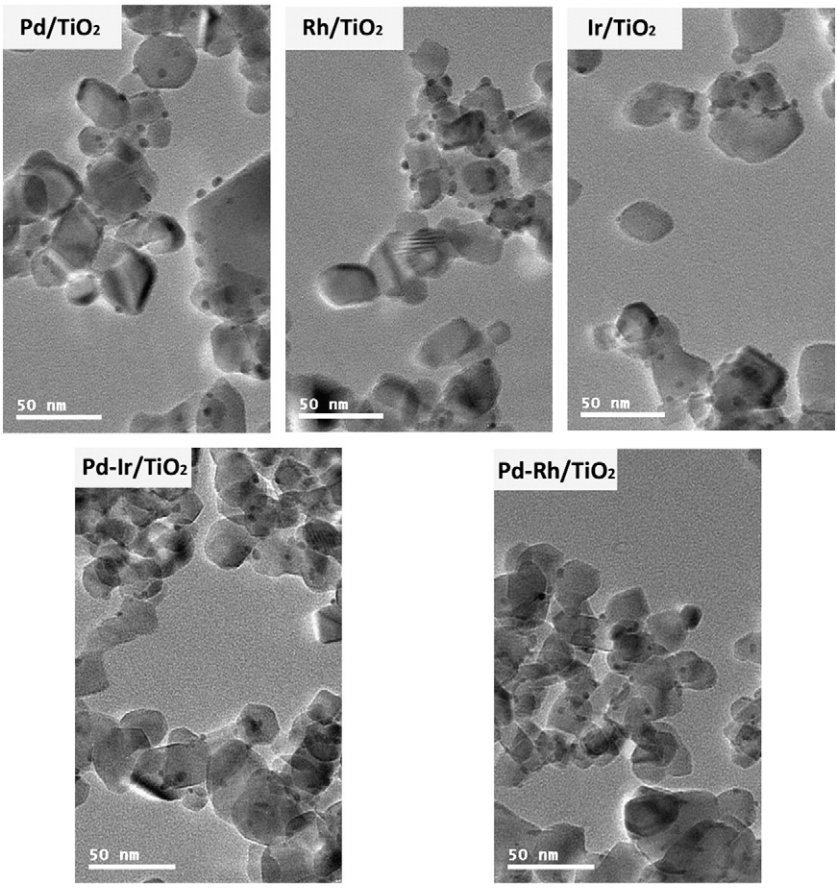

Fig. 1. TEM images of TiO_2 supported catalysts.

at 100 mL/min and the typical reactant gas composition consisted of 1000 ppm NO, 3000 ppm H_2, 5% O_2 and the balance He. A sample weight of 100 mg (ca. 0.1 cm^3) was employed, corresponding to the gas hourly space velocity (GHSV) of 60000/h. The products were analyzed on-line by using a gas chromatograph (Varian CP 3800, for H_2, N_2, NH_3 and N_2O analysis) and a chemiluminescence NO_x analyzer (Ecotech EC 9841, for NO and NO_2 analysis). The NO_x conversion is calculated as $([NO]_{inlet} - [NO]_{outlet} - [NO_2]_{outlet})/[NO]_{inlet} * 100\%$ and the N_2 selectivity is calculated as $2\,[N_2]_{outlet}/[NO]_{inlet} * 100\%$.

2.4. In situ FTIR studies

In situ FTIR spectra were recorded on the Bruker Tensor 27 spectrometer, equipped with a liquid N_2 cooled highly sensitive MCT detector. The catalyst samples of ca. 25 mg were finely ground and placed in the reaction chamber. Prior to each experiment, the sample was pretreated in He at 573 K for 1 h, and cooled to the desired temperature for taking a reference spectrum. Then, the reaction gas mixture (1000 ppm NO, 3000 ppm H_2, 5% O_2, He balance) was fed to the sample and the steady-state spectra were recorded with a resolution of 4 cm^{-1} and an accumulation of 128 scans.

3. Results and discussion

3.1. Characterization results

The typical TEM images of TiO_2 supported catalysts are shown in Fig. 1. For monometallic catalysts, supported metal clusters with averages diameters of 4–6 nm are evenly dispersed on the surface of TiO_2 support. For bimetallic catalysts, metal clusters with slightly smaller sizes are observed. However, the TEM images cannot give exact information on whether bimetallic clusters or islands of monometallic clusters are formed. The physical–chemical properties of TiO_2 supported catalysts are summarized in Table 1.

3.2. Catalytic results

The catalytic performances of TiO_2 supported monometallic and bimetal catalysts in H_2-SCR reaction are displayed in Fig. 2. TiO_2 supported monometallic catalysts are active in H_2-SCR reaction and the H_2-SCR activity is observed as $Ir/TiO_2 > Pd/TiO_2 > Rh/TiO_2$. The H_2 conversions increase with reaction temperature and reach 100% at 423, 523 and 548 K over Pd/TiO_2, Ir/TiO_2 and Rh/TiO_2, respectively. Pd species are highly active for H_2 activation, while Rh and Ir species are highly active for NO dissociative activation [16,17]. Therefore, we try to combine the functions of Pd with Rh or Ir to improve the H_2-SCR catalytic performance. As expected, strong synergistic effects exist between Pd and Ir, and excellent deNO_x activity can be obtained on bimetallic Pd–Ir/TiO_2. Typically, NO_x conversion of >80%, with N_2

Table 1
Physical–chemical properties of TiO_2 supported catalysts.

Catalyst	Surface area	Metal loading[a]	Metal size[b]	Metal dispersion[c]
Pd/TiO_2	44 m^2/g	Pd: 1.9%	5.4 nm	36%
Rh/TiO_2	46 m^2/g	Rh: 1.8%	4.5 nm	32%
Ir/TiO_2	46 m^2/g	Ir: 1.7%	4.7 nm	37%
Pd–Ir/TiO_2	45 m^2/g	Pd: 0.9%; Ir: 0.8%	4.1 nm	39%
Pd–Rh/TiO_2	46 m^2/g	Pd: 0.9%; Rh: 0.9%	4.2 nm	41%

[a] Determined by ICP-AES.
[b] Average size observed by TEM.
[c] Determined by H_2 chemisorption.

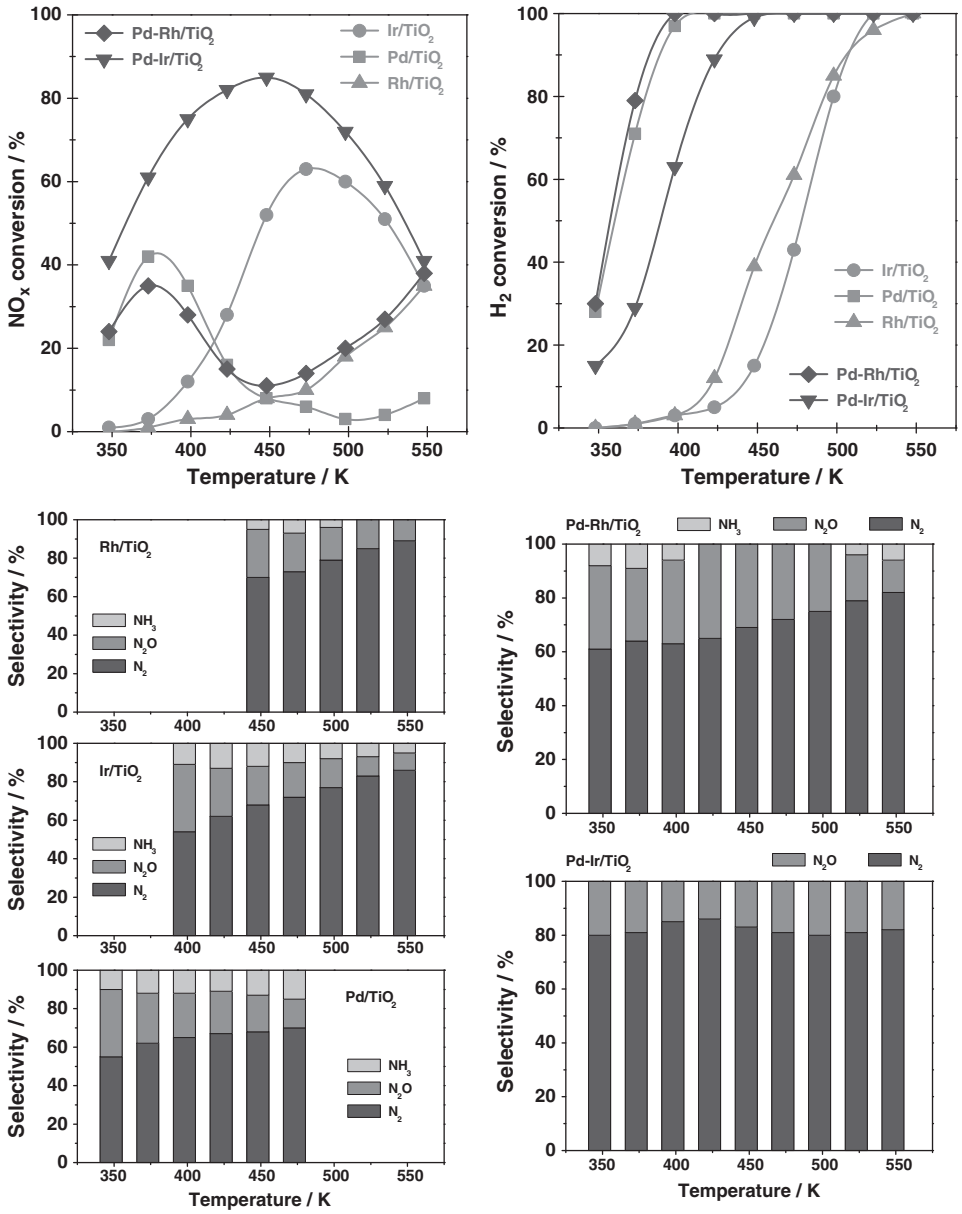

Fig. 2. Catalytic performances of TiO_2 supported catalysts for NO selective reduction by hydrogen. Reaction conditions: NO = 1000 ppm. H_2 = 3000 ppm, O_2 = 5%; GHSV = 60,000/h.

selectivity >80%, is observed within the temperature range of 413–473 K. It is worth mentioning that the catalytic performances of Pd–Ir/TiO_2 for H_2-SCR reaction are comparable with most active Pt catalysts reported in literature under similar conditions [3]. In contrast, the synergistic effects between Pd and Rh are not so obvious, and bimetallic Pd–Rh/TiO_2 does not exhibit improved deNO_x activity compared with monometallic Pd/TiO_2 and Rh/TiO_2.

3.3. Existence states of supported metals before and after H_2-SCR

The changes in states of supported metals before and after H_2-SCR reaction were investigated by means of XPS, and the results are shown in Fig. 3. For Pd/TiO_2 before reaction, the peaks of binding energy are observed at 335.1 and 340.4 eV, corresponding to the Pd $3d_{5/2}$ and Pd $3d_{3/2}$, respectively [18]. After H_2-SCR at 423 K, both metallic Pd^0 (335.1 and 340.4 eV) and ionic Pd^{2+} (337.1 and 342.4 eV) can be observed. It is quite clear that palladium species in Pd/TiO_2 are partially oxidized during H_2-SCR reaction at 423 K, which may be the key reason for the low H_2-SCR activity at this temperature. For Ir/TiO_2 before reaction, the peaks of binding energy are observed at 60.1 and 63.1 eV, corresponding to the Ir $4f_{7/2}$ and Ir $4f_{5/2}$, respectively. After H_2-SCR at 423 K, iridium species are partially oxidized, and both metallic Ir^0 (60.1 and 63.1 eV) and $Ir^{\delta+}$ (61.9 and 64.7 eV) can be observed [19]. For Pd–Ir/TiO_2 before reaction, palladium species exist in the form of Pd^0 and iridium species exist in the form of Ir^0. After H_2-SCR reaction, the metallic form of palladium and iridium in Pd–Ir/TiO_2 are well preserved, in great contrast to Pd/TiO_2 and Ir/TiO_2. This may be due to the synergistic effects between Pd and Ir, which also lead the high H_2-SCR activity of Pd–Ir/TiO_2.

3.4. In situ FTIR studies of H_2-SCR on Pd/TiO_2, Ir/TiO_2 and Pd–Ir/TiO_2

FTIR spectra of adsorbed species formed on the surface of Ir/TiO_2, Pd/TiO_2 and Pd–Ir/TiO_2 catalysts under H_2-SCR reaction conditions are shown in Fig. 4, and the concise assignments of IR bands are summarized in Table 2.

Under H_2-SCR reaction conditions, predominant various N_xO_y species are formed on Pd/TiO_2, as indicated by the appearance of multiple

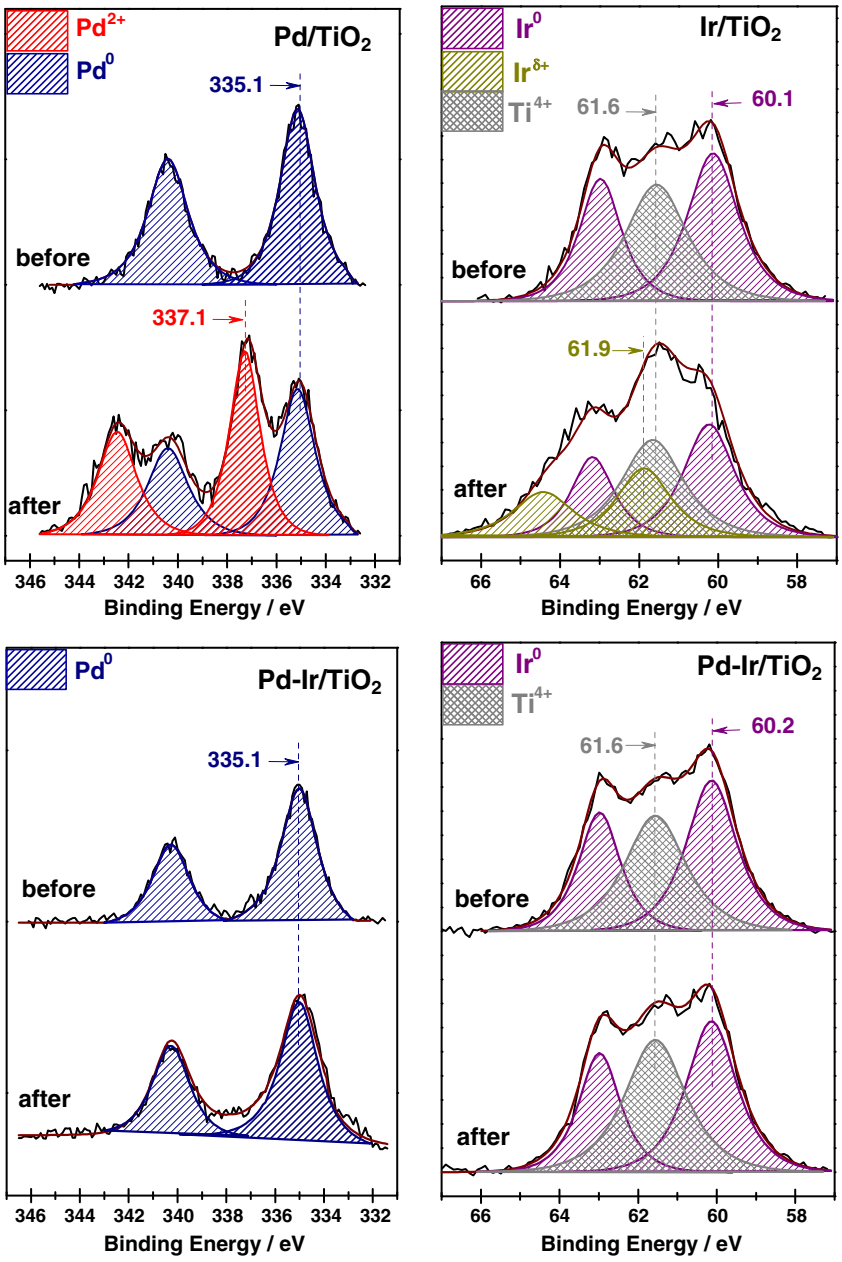

Fig. 3. XPS of Ir/TiO_2, Pd/TiO_2 and $Pd–Ir/TiO_2$ before and after H_2-SCR reaction at 423 K for 6 h.

bands at below 1640 cm^{-1}. Specifically, the band at 1605 cm^{-1} is assigned to bridging bidentate nitrate species, while the bands at 1580 and 1300 cm^{-1} are assigned to chelating bidentate nitrate species on TiO_2. The band 1485 cm^{-1} is assigned to mono-dentate nitrate species and the band at 1520 cm^{-1} is assigned to nitro species [20,21]. Besides, IR band at 1250 cm^{-1} corresponding to NH_3 on Lewis acid sites, accompanied by IR bands at 3100–3400 cm^{-1} corresponding to the NH stretching modes, can be observed [22], indicating the formation NH_3 during H_2-SCR reaction. Considering that the reaction between NH_3 and NO occurs at temperature higher than 473 K [12], the NH_3 is released as by-product at temperature below 473 K (ref. Fig. 2). Mono-nitrosyl on Pd^0 (band at 1745 cm^{-1}) and Pd^{n+} (band at 1775 cm^{-1}) [20], are detected during H_2-SCR reaction at 373 K, indicating the existence of both Pd^0 and Pd^{n+} at this temperature. Some metallic Pd^0 species are gradually oxidized to cationic Pd^{n+} with increasing reaction temperature up to 473 K. Considering that H_2 preferentially adsorbs on palladium sites over NO, the major pathway for H_2-SCR over Pd/TiO_2 at low temperatures is proposed to be hydrogen assisted NO dissociation and subsequent nitrogen formation ($NO + 2H_{ad} \rightarrow H_2O + N_{ad}$; $N_{ad} + N_{ad} \rightarrow N_2$). The by-product N_2O should come from the combination of adsorbed N and gaseous NO ($NO + N_{ad} \rightarrow N_2O$) and the by-product NH_3 should come from the hydrogenation of adsorbed N ($N_{ad} + 3H_{ad} \rightarrow NH_3$).

Under H_2-SCR reaction conditions, various N_xO_y species are formed on Ir/TiO_2 at 373–473 K. At 373 K, mono-nitrosyl on Ir^0 (band at 1880 cm^{-1}) and $Ir^{\delta+}$ (band at 1910 cm^{-1}) [24] are detected during H_2-SCR reaction. With increasing temperatures, the $Ir^{\delta+}$ species are gradually reduced to Ir^0, as suggested by the disappearance of IR band at 1910 cm^{-1} and the increase in the intensity of IR band at 1880 cm^{-1}. The high activity of Ir/TiO_2 at higher reaction temperatures is a consequence of iridium existing in metallic form during H_2-SCR reaction. Considering that NO preferentially adsorbs on palladium sites over H_2, the major H_2-SCR pathway over Ir/TiO_2 should be the dissociation of NO and subsequent recombination of adsorbed N ($NO \rightarrow N_{ad} + O_{ad}$; $N_{ad} + N_{ad} \rightarrow N_2$) [17]. The function of hydrogen is assisting the removal of adsorbed O ($H_2 + O_{ad} \rightarrow H_2O$).

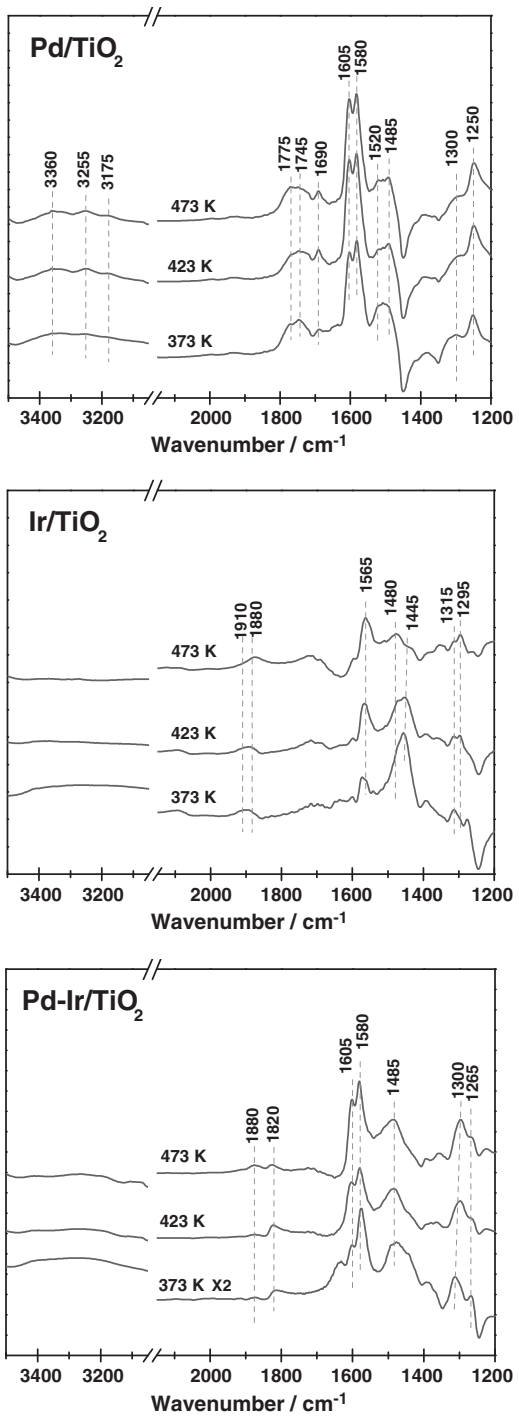

Fig. 4. FTIR spectra of adsorbed species formed on surface of Ir/TiO_2, Pd/TiO_2 and $Pd–Ir/TiO_2$ catalysts under H_2-SCR reaction conditions.

The by-product N_2O should come from the combination of adsorbed N and adsorbed NO ($NO_{ad} + N_{ad} \rightarrow N_2O$) and the by-product NH_3 should come from the reaction between adsorbed N and gaseous hydrogen ($2N_{ad} + 3H_2 \rightarrow 2NH_3$).

For bimetallic $Pd–Ir/TiO_2$ under H_2-SCR conditions, similar N_xO_y species (bridging bidentate nitrates at 1605 cm^{-1}; chelating bidentate nitrates at 1580 and 1300 cm^{-1}; monodentate nitrates at 1485; and mono-dentate nitrites at 1265 cm^{-1}) are formed on the surface of TiO_2. Besides, mono-nitrosyl on Ir^0 particles (band at 1880 cm^{-1}) and well defined Ir^0 nitrosyl complexes (band at 1820 cm^{-1}) are observed [25], indicating that Ir species exist in metallic form in bimetallic $Pd–Ir/TiO_2$ in the temperature range studied. Obviously, the addition of Pd species to Ir/TiO_2 greatly suppresses the oxidation of Ir species during reaction, in great consistent with XPS results. The observations from in situ FTIR spectra confirm that the adsorption and activation of NO occur on Ir sites. Therefore, the major H_2-SCR pathway over $Pd–Ir/TiO_2$ is essentially the same as that over Ir/TiO_2, i.e. the dissociation of NO and subsequent recombination of adsorbed N ($NO \rightarrow N_{ad} + O_{ad}$; $N_{ad} + N_{ad} \rightarrow N_2$). The dissociation of H_2 occurs on Pd sites and the adsorbed H on Pd sites facilitates the removal of adsorbed O on Ir sites through hydrogen spillover ($2H_{ad} + O_{ad} \rightarrow H_2O$). The reaction between N_{ad} and gaseous H_2 on Ir sites ($2N_{ad} + 3H_2 \rightarrow 2NH_3$) is totally suppressed, and therefore, N_2O is observed as the only by-product from H_2-SCR over $Pd–Ir/TiO_2$ (ref. selectivity data in Fig. 2).

Table 2
Assignments of IR bands observed during H_2-SCR reaction.

Catalyst	Wavenumber	Assignment
Pd/TiO_2	1250 cm^{-1}	NH_3 on Lewis acid sites
	1300 and 1580 cm^{-1}	Chelating bidentate nitrates
	1485 cm^{-1}	Mono-dentate nitrates
	1520 cm^{-1}	Chelating nitro species
	1605 cm^{-1}	Bridging bidentate nitrates
	1690 cm^{-1}	Bent Pd–NO species [23]
	1745 cm^{-1}	Mono-nitrosyl on Pd^0
	1775 cm^{-1}	Mono-nitrosyl on Pd^{n+}
	3100–3400 cm^{-1}	NH stretching modes
Ir/TiO_2	1295 and 1565 cm^{-1}	Chelating bidentate nitrates
	1445 cm^{-1}	Mono-dentate nitro species [20]
	1315 cm^{-1}	Hyponitrites
	1480 cm^{-1}	Mono-dentate nitrates
	1880 cm^{-1}	Mono-nitrosyl on Ir^0
	1910 cm^{-1}	Mono-nitrosyl on $Ir^{\delta+}$
$Pd–Ir/TiO_2$	1265 cm^{-1}	Mono-dentate nitrites
	1300 and 1580 cm^{-1}	Chelating bidentate nitrates
	1485 cm^{-1}	Mono-dentate nitrates
	1605 cm^{-1}	Bridging bidentate nitrates
	1820 cm^{-1}	Nitrosyl complexes on Ir^0 particles
	1880 cm^{-1}	Mono-nitrosyl on Ir^0

4. Conclusion

TiO_2 supported monometallic and bimetallic catalysts, i.e. Pd/TiO_2, Ir/TiO_2, Rh/TiO_2, $Pd–Ir/TiO_2$ and $Pd–Rh/TiO_2$, were studied for H_2-SCR reaction. Synergistic effects between Pd and Ir were formed on $Pd–Ir/TiO_2$, while no synergistic effects between Pd and Rh were formed on $Pd–Rh/TiO_2$. Therefore, $Pd–Ir/TiO_2$ exhibited high activity, much greater than the sum of Pd/TiO_2 and Ir/TiO_2, in H_2-SCR reaction. On the one hand, the presence of Pd greatly suppressed the oxidation of Ir species during reaction. On the other hand, the adsorbed hydrogen on Pd sites promoted the removal of adsorbed oxygen on Ir sites through spillover.

Acknowledgments

This work is financially supported by the National Natural Science Found of China (20973094), the Research Fund for the Doctoral Program of Higher Education of China (20100031120014), and the NCET11-0251 of Ministry of Education and the State Key Laboratory of Engines (K2011-02).

References

[1] R.M. Heck, Catalysis Today 53 (1999) 519.
[2] Z.M. Liu, S.I. Woo, Catalysis Reviews: Science and Engineering 48 (2006) 43.
[3] P.G. Savva, C.N. Costa, Catalysis Reviews: Science and Engineering 53 (2011) 91.
[4] C.N. Costa, V.N. Stathopoulos, V.C. Belessi, A.M. Efstathiou, Journal of Catalysis 197 (2001) 350.
[5] J. Shibata, M. Hashmoto, K. Shimizu, H. Yoshida, T. Hattori, A. Satsuma, The Journal of Physical Chemistry. B 108 (2004) 18327.
[6] S. Hamada, K. Ikeue, M. Machida, Applied Catalysis B: Environmental 71 (2006) 1.

[7] C.N. Costa, A.M. Efstathiou, Applied Catalysis B: Environmental 72 (2007) 240.
[8] A. Tomita, T. Yoshii, S. Teranishi, M. Nagao, T. Hibino, Journal of Catalysis 247 (2007) 137.
[9] L. Li, P. Wu, Q. Yu, G. Wu, N. Guan, Applied Catalysis B: Environmental 94 (2010) 254.
[10] P. Wu, L. Li, Q. Yu, G. Wu, N. Guan, Catalysis Today 158 (2010) 228.
[11] A. Ueda, T. Nakato, M. Azuma, T. Kobayashi, Catalysis Today 45 (1998) 135.
[12] N. Macleod, R. Cropley, R.M. Lambert, Catalysis Letters 86 (2003) 69.
[13] G. Qi, R.T. Yang, F.C. Rinaldi, Journal of Catalysis 237 (2006) 381.
[14] L. Li, F. Zhang, N. Guan, E. Schreier, M. Richter, Catalysis Communications 9 (2008) 1827.
[15] L. Liu, X. Guan, Z. Li, X. Zi, H. Dai, H. He, Applied Catalysis B: Environmental 90 (2009) 1.
[16] B. Hammer, J.K. Norskov, Advances in Catalalysis 45 (2000) 71.
[17] Z.P. Liu, S.J. Jenkins, D.A. King, Journal of the American Chemical Society 126 (2004) 10746.
[18] C.D. Wagner, W.M. Riggs, L.E. Davis, J.F. Moulder, G.E. Muilenberg, Handbook of X-ray Photoelectron Spectroscopy: A Reference Book of Standard Data for Use in X-ray Photoelectron Spectroscopy, Eden-Prairie, Perkin-Elmer MN, 1979.
[19] W. Feng, G. Wu, L. Li, N. Guan, Green Chemistry 13 (2011) 3265.
[20] K. Hadjiivanov, Catalysis Reviews: Science and Engineering 42 (2000) 71.
[21] M.A. Debeila, N.J. Coville, M.S. Scurrell, G.R. Hearne, Journal of Molecular Catalysis A: Chemical 219 (2004) 131.
[22] M.A. Centeno, M. Debois, P. Grange, The Journal of Physical Chemistry. B 102 (1998) 6835.
[23] K. Almusaiteer, S.S.C. Chuang, Journal of Catalysis 184 (1999) 189.
[24] G.B. McVicker, R.T.K. Baker, R.L. Garten, E.L. Kugler, Journal of Catalysis 65 (1980) 207.
[25] E. Iojoiu, P. Gélin, H. Praliaud, M. Primet, Applied Catalysis A: General 263 (2004) 39.